Multi-channel Images derived Priors for Image Restoration and Reconstruction

Qiegen Liu

Department of Electronic Information Engineering

Nanchang University

Nanchang 330031, China

MICS 2019: July 13-14, 2019 - Suzhou, China

Joint work with
Dong Liang,
Henry Leung,
Shanshan Wang,
Binjie Qin,
Minghui Zhang ,
Yuhao Wang,
and
master Students
Hongyang Lu
Jiaojiao Xiong
Sanqian Li
Fengqin Zhang
Qinxin Yang
Wenzhao Zhao

Outline

Target: How to ultilize higher-dimensional prior in reconstruction ?

Motivation: 1. Network for color-to-grayscale (TIP, INFFUS)
2. Multi-filters guided tensor for image Rec (TMM)

Works: 1. Ultilizing prior in color space to grayscale IR (TIP)
2. Utilizing self-copy prior in MR Rec (MRM)
3. Ultilizing color/multi-coil MR prior to CT Rec (TMI)

Conclusions

Target: How to ultilize higher-dimensional prior in reconstruction ?

Color images

Color prior knowledge

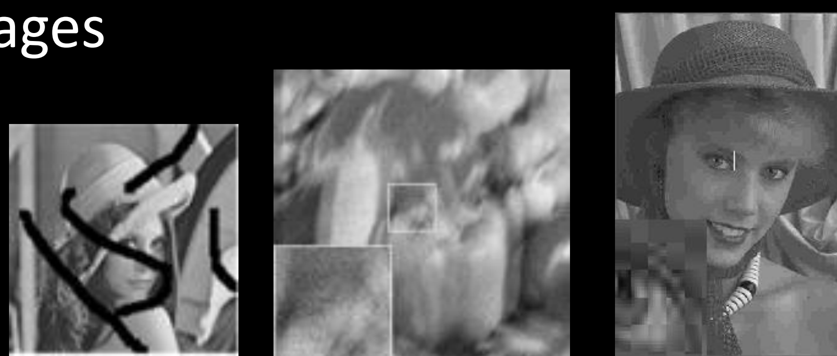

Grayscale images

Target: How to ultilize higher-dimensional prior in reconstruction ?

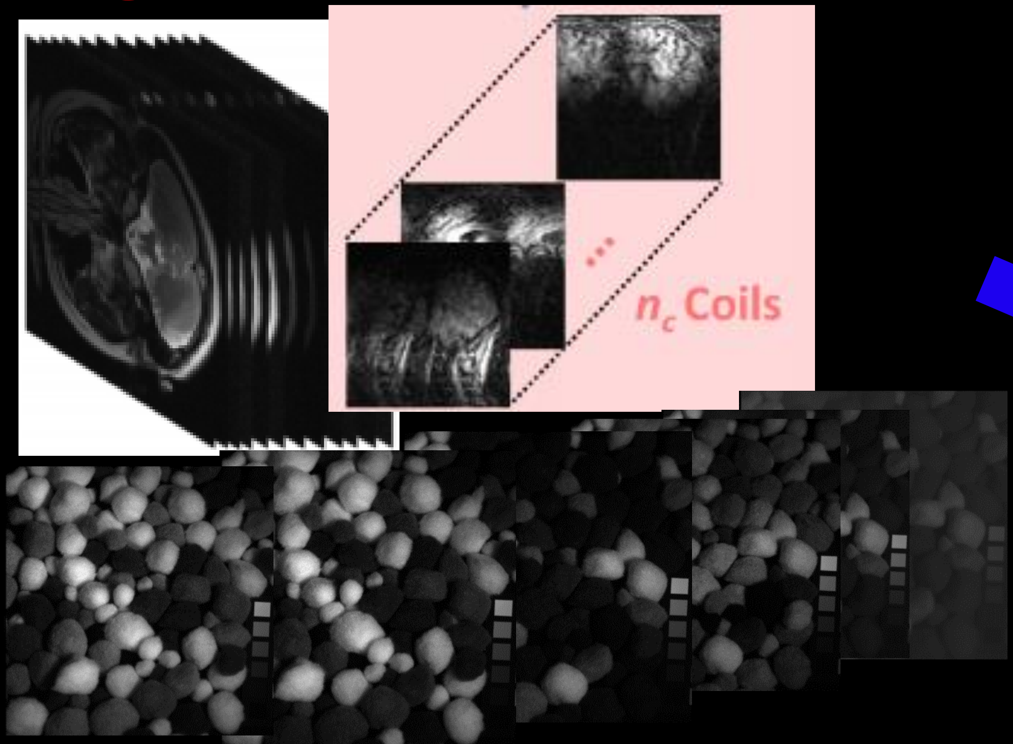

Multi-coil MR images, Hyperspectral images, ….

Multi-channel prior knowledge

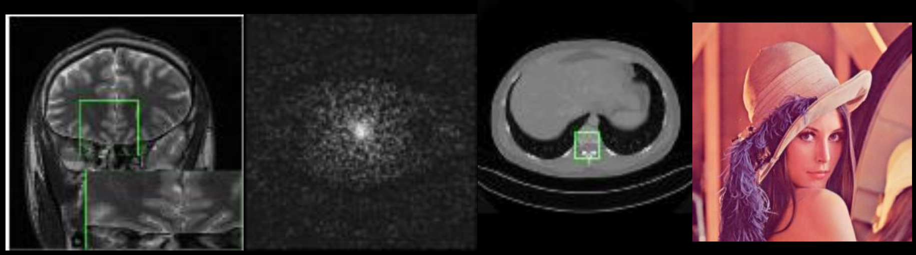

Single-coil MR/CT images, Color images

Part I-1 – Motivation

from

color-to-grayscale problem

Decolorization (color-to-grayscale)

color image I *three-channels* I_r I_g I_b *single-channel grayscale image* g

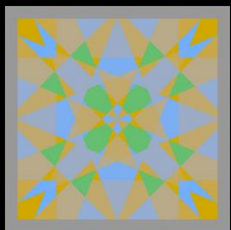

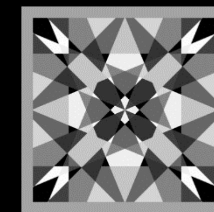

Conventional strategies

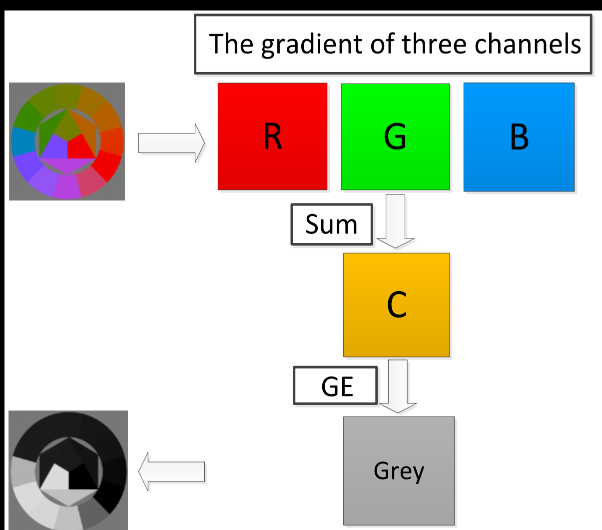

$$\min_{g} \sum_{(x,y)\in P} (g_x - g_y - \delta_{x,y})^2, \qquad \left|\delta_{x,y}\right| = \sqrt{\sum_{c=\{r,g,b\}} (I_{c,x} - I_{c,y})^2}$$

$$\min_{g} \; -\sum_{(x,y)\in P} \ln\{\alpha_{x,y} N_{\sigma}(g_x - g_y + \delta_{x,y}) + (1-\alpha_{x,y}) N_{\sigma}(g_x - g_y - \delta_{x,y})\}$$

....

Many of them are based on the gradient error (GE) measure, calculated in the single-channel data space.

Refs: Gooch et al. 2005; Kim et al., 2009; Kuk et al., 2010; Lu et al., 2012; Song et al, 2010; Lu et al, 2012.

GcsDecolor (Gradient Correlation Similarity)

Our strategy

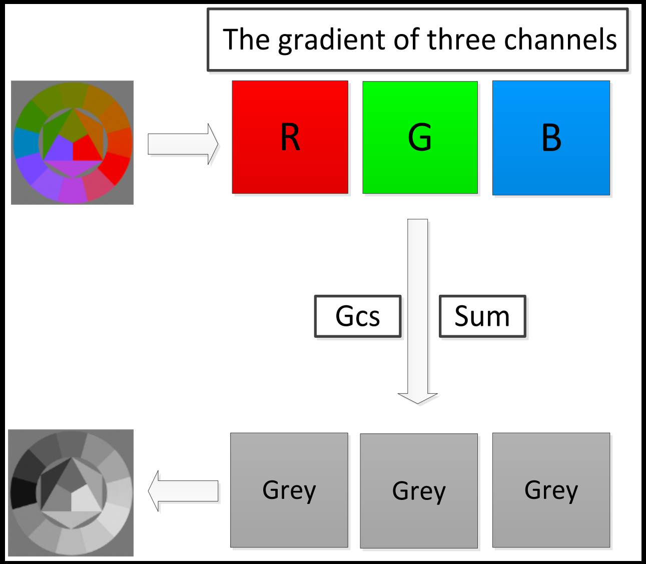

$$\min_{w_c} -\sum_{(x,y)\in P}\sum_{c=\{r,g,b\}}\frac{2\left|I_{c,x}-I_{c,y}\right|\left|\nabla g_{x,y}\right|}{\left|I_{c,x}-I_{c,y}\right|^2+\left|\nabla g_{x,y}\right|^2}$$

The proposed measure adaptively calculates the gradient correlation for each channel rather than the whole channels at one time. It is calculated in the three-channel data space.

Gcs measure computes the overall pixel-wise similarity between the gradient magnitudes in each channel of the original color image and the resulting grayscale image

Qiegen Liu, Xiaoping Liu, Weisi Xie, Yuhao Wang, Dong Liang. GcsDecolor: Gradient correlation similarity for efficient contrast preserving decolorization, ***IEEE Trans. Image Process.***, vol. 24, no. 9, pp. 2889-2904, 2015.

GcsDecolor (Gradient Correlation Similarity)

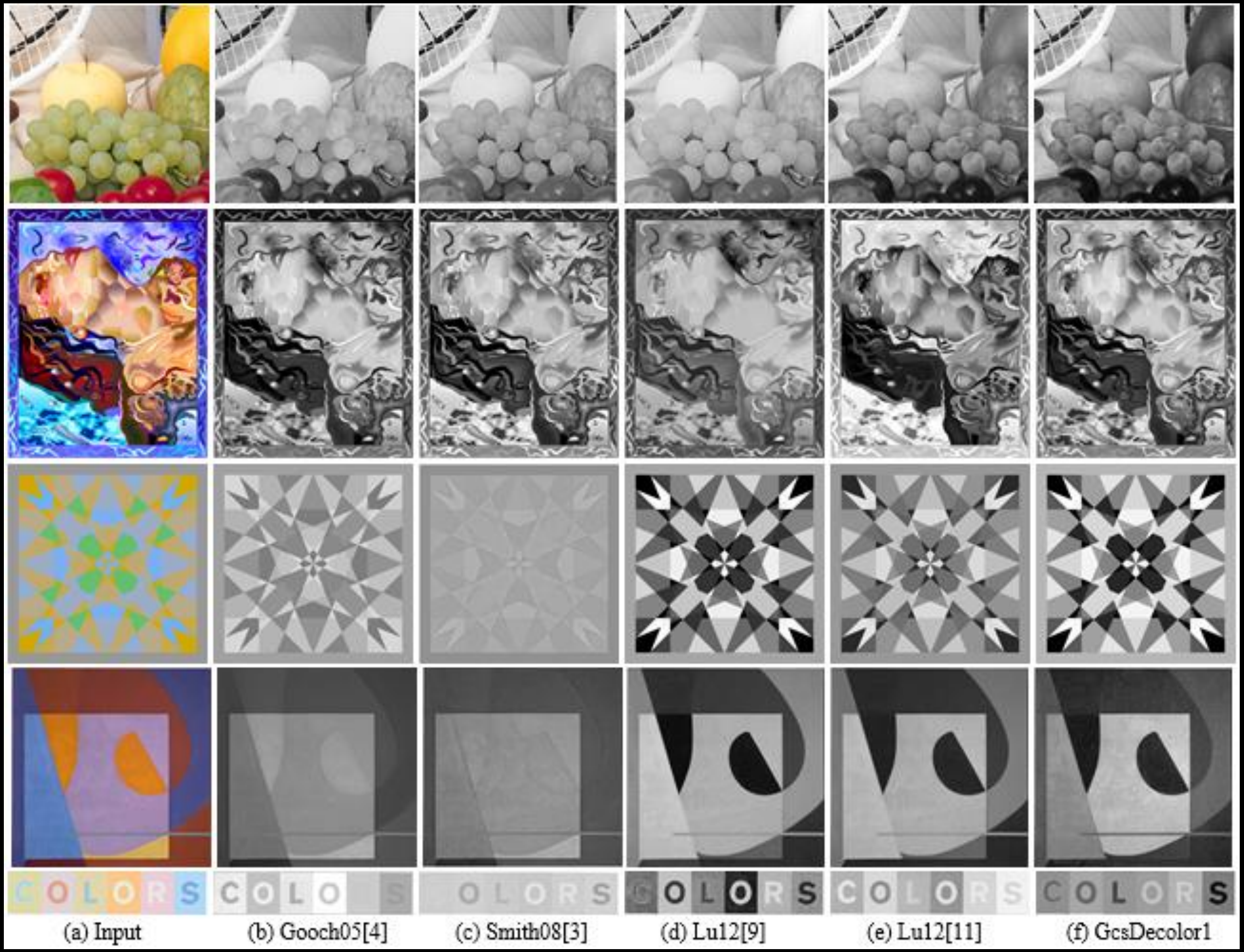

Some results

Qiegen Liu, Xiaoping Liu, Weisi Xie, Yuhao Wang, Dong Liang. GcsDecolor: Gradient correlation similarity for efficient contrast preserving decolorization, ***IEEE Trans. Image Process.***, vol. 24, no. 9, pp. 2889-2904, 2015.

DecolorNet (Network for Decolorization)

Similar to Gcs, we introduce the L1-norm with variable augmentation technique:

Cost function of the network: $\min_{w} \left| F_w(\nabla I) - \nabla G \right|_1$

where $I = \{I_R, I_G, I_B\}$ and $G = \{g, g, g\}$ is an auxiliary variable.

$F_w(\bullet)$ is the network that we need to design and train.

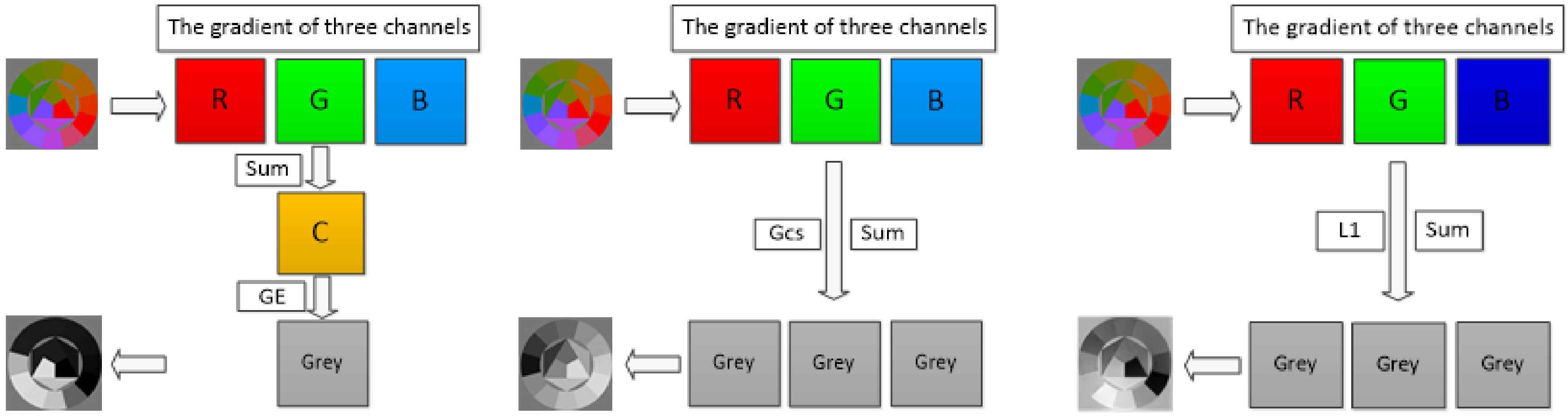

(a) (b) (c)

Fig. 10. Example confirming the auxiliary variables technique. (a) GE measure. (b) Gcs measure. (c) Proposed L1-norm measure.

Q. Liu, H. Leung, "Variable augmented neural network for decolorization and multi-exposure fusion," *Information Fusion*, vol. 46, pp.114-127, 2019.

DecolorNet (Network for Decolorization)

Network design

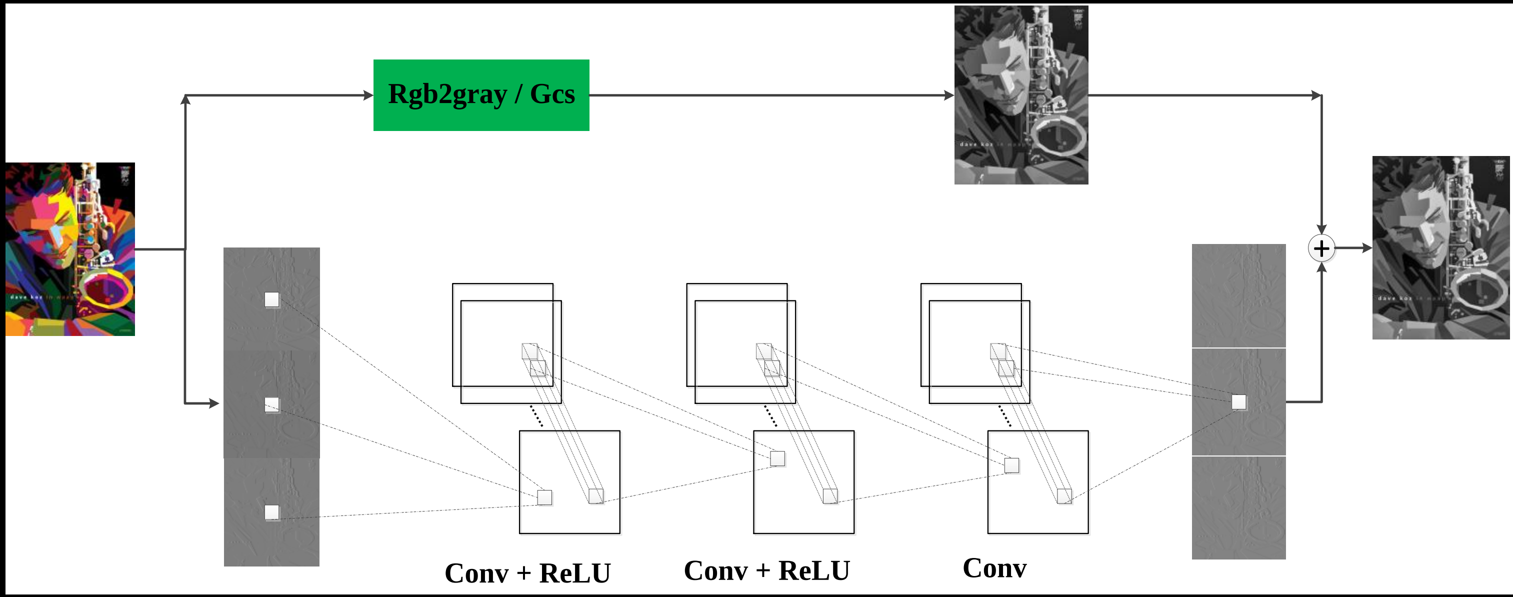

Demonstration the flowchart of the proposed DecolorNet architecture.

The proposed network is formulated as a shallow and easily-trainable CNN:

$$F_0(\partial I) = \partial I, n = 0$$

$$F_w^n(\partial I) = \sigma(W^n * F_w^{n-1}(\partial I) + b^n), n = 1, 2$$

$$F_w(\partial I) = W^n * F_w^{n-1}(\partial I) + b^n, n = 3$$

Q. Liu, H. Leung, "Variable augmented neural network for decolorization and multi-exposure fusion," *Information Fusion*, vol. 46, pp.114-127, 2019.

DecolorNet (Network for Decolorization)

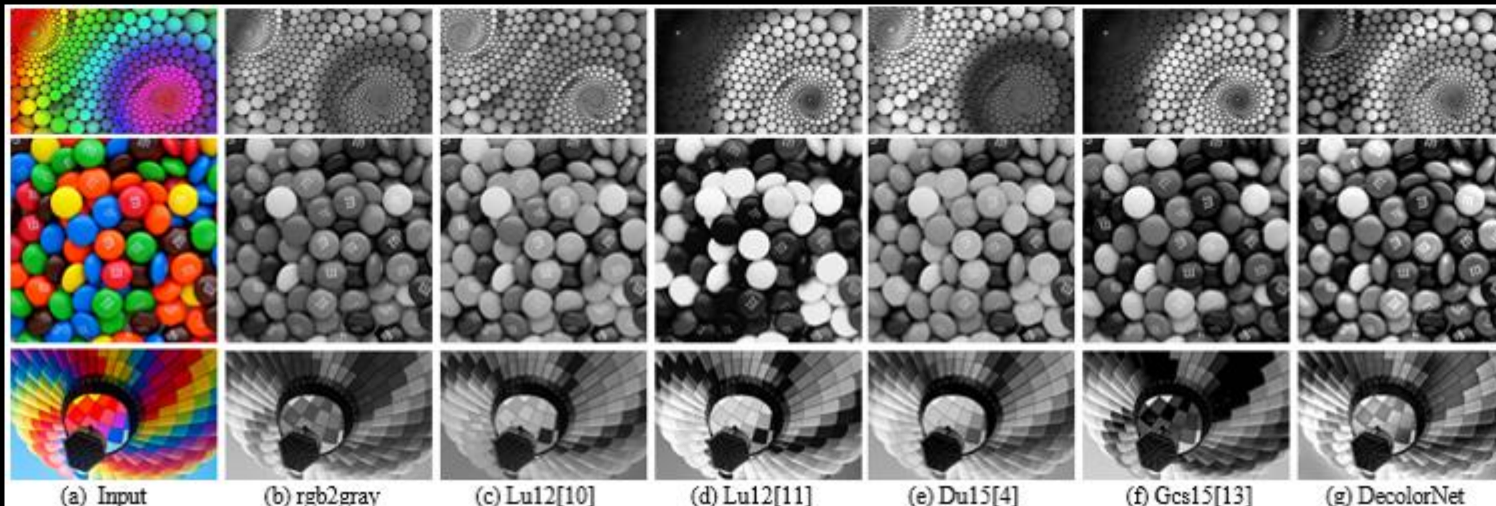

Decolorization

Multi-exposure image fusion: FusionNet

Q. Liu, H. Leung, "Variable augmented neural network for decolorization and multi-exposure fusion," *Information Fusion*, vol. 46, pp.114-127, 2019.

Part I-2 – Motivation

from

Multi-filters guided tensor optimization for image restoration

Field-of-Experts Filters Guided Tensor Completion

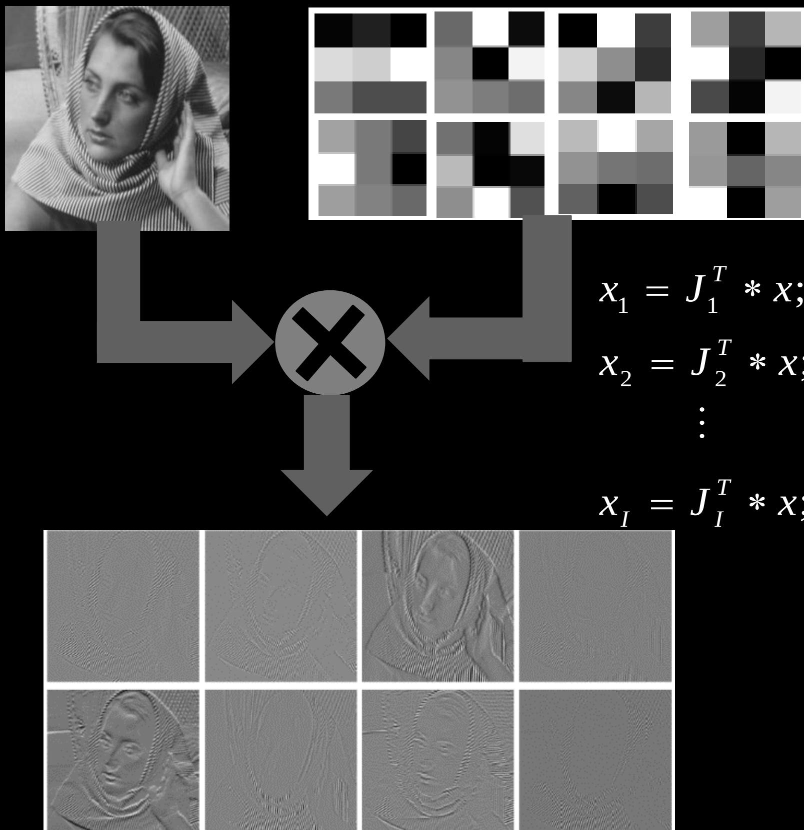

$$x_1 = J_1^T * x;$$
$$x_2 = J_2^T * x;$$
$$\vdots$$
$$x_I = J_I^T * x;$$

Multi-view features seamlessly contain rich information such as high-frequency information, edges and textures at various orientations and scales.

Proposition 1. $\left\| [J_1^T, \cdots, J_I^T] * \mathcal{X} \right\|_* \le \sum_{i=1}^{I} \left\| J_i^T * \mathcal{X} \right\|_*$

Proposition 2. $\left\| J_i^T * \mathcal{X} \right\|_* \le \left\| \mathcal{X} \right\|_*, \quad \forall i$

Considering a color image "Barbara" $\mathcal{X}$ and its one-FoE filter resulting tensor $J_1^T * \mathcal{X}$

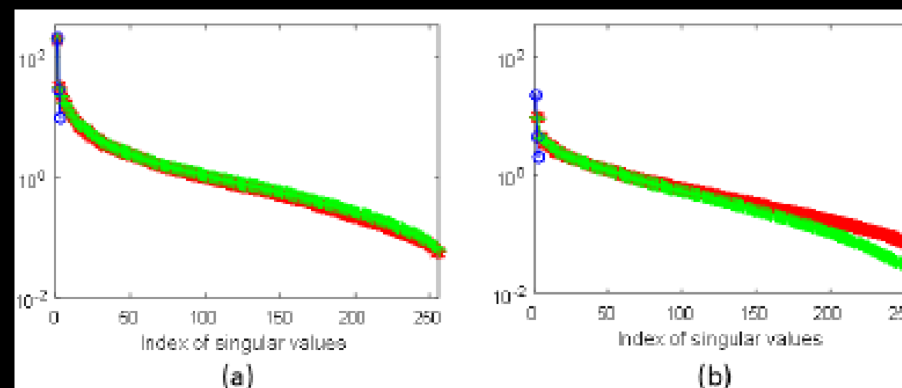

Singular values of three unfolding matrices of (a) the original tensor "Barbara" with size 256×256× 3, and (b) the associated feature tensor.

Ref. [1] S. Roth, and M. J. Black, "Fields of Experts," *IJCV*, 2009.
[2] U. Schmidt and S. Roth, "Shrinkage fields for effective image restoration," in *CVPR*, 2014.

Field-of-Experts Filters Guided Tensor Completion

FoE-STDC:

Incorporate the FoE filters into the STDC model (Chen *et al.*, "Simultaneous tensor decomposition and completion using factor priors," IE*EE TPAMI*, 2014), it yields:

Algorithm 2 FoE-STDC

Input : an incomplete tensor $\mathcal{X}_0 \in \mathbb{R}^{I_1 \times I_2 \times \ldots \times I_n}$, matrix $\mathbf{L}$

Initialize $\mathcal{X}, \mathrm{V}_1^1, ..., \mathrm{V}_\mathrm{n}^1, \mathrm{V}_1^2, ..., \mathrm{V}_\mathrm{n}^2, \mathcal{Z}_1, \mathcal{Z}_2, \mathcal{Y}_1, \mathcal{Y}_2, \mathcal{B}, \mathcal{W}$ by V_k: identity matrix $(1 \le \mathrm{k} \le \mathrm{n})$, $\mathcal{Z} = \mathcal{X} = \mathcal{X}_0$ and $\mathcal{Y} = 0$

For $t = 1, 2, \cdots$, repeat until a stop-criterion is satisfied

updata V_k^1 and V_k^2 via Eq. (19)

updata $\mathcal{Z}_1$ and $\mathcal{Z}_2$ via Eq. (21)

updata $\mathcal{B}$ via Eq. (23)

updata $\mathcal{X}$ via Eq. (25)

updata $\mathcal{Y}_1$ and $\mathcal{Y}_2$ via

$$\mathcal{Y}_1^{t+1} = \mathcal{Y}_1^t + \mu_1^t(\mathcal{X} - \mathcal{Z}_1 \times_1 \mathrm{V}_1^{1T} \ldots \times_n \mathrm{V}_\mathrm{n}^{1T})$$
$$\mathcal{Y}_2^{t+1} = \mathcal{Y}_2^t + \mu_2^t(\mathcal{B} - \mathcal{Z}_2 \times_1 \mathrm{V}_1^{2T} \ldots \times_n \mathrm{V}_\mathrm{n}^{2T})$$

updata $\mathcal{W}$ via

$$\mathcal{W}_1^{t+1} = \mathcal{W}_1^t + \lambda^t(\mathcal{B} - [J_1^T, ..., J_I^T] * \mathcal{X})$$

$\mu_1^{t+1} = \rho\mu_1^t, \mu_2^{t+1} = \rho\mu_2^t, \rho \in [1.1, 1.2]$

End

Output: $\mathcal{X}, \mathrm{V}_1^1, ..., \mathrm{V}_\mathrm{n}^1, \mathrm{V}_1^2, ..., \mathrm{V}_\mathrm{n}^2, \mathcal{Z}_1, \mathcal{Z}_2$ and $\mathcal{B}$

$$\min_{\mathcal{X}, \mathcal{Z}_1, \mathcal{Z}_2, \mathbf{V}_1^1, \cdots, \hat{\mathbf{V}}_\mathrm{n}^1, \mathbf{V}_1^2, \cdots, \mathbf{V}_\mathrm{n}^2} \sum_{\mathrm{k}=1}^{\mathrm{n}} \alpha_\mathrm{k}^1 \|\mathbf{V}_\mathrm{k}^1\|_* + \beta_1 tr((\mathbf{V}_1^1 \otimes \cdots \otimes \mathbf{V}_\mathrm{n}^1)\mathbf{L}(\mathbf{V}_1^1 \otimes \cdots \otimes \mathbf{V}_\mathrm{n}^1)^T) + \gamma_1 \|\mathcal{Z}_1\|_F^2$$

$$+\eta(\sum_{\mathrm{k}=1}^{\mathrm{n}} \alpha_\mathrm{k}^2 \|\mathbf{V}_\mathrm{k}^2\|_* + \gamma_2 \|\mathcal{Z}_2\|_F^2 + \beta_2 tr((\mathbf{V}_1^2 \otimes \cdots \otimes \mathbf{V}_\mathrm{n}^2)\mathbf{L}(\mathbf{V}_1^2 \otimes \cdots \otimes \mathbf{V}_\mathrm{n}^2)^T)$$

$$\text{s.t.}\ \mathcal{X} = \mathcal{Z}_1 \times_1 \mathbf{V}_1^{1\mathrm{T}} \cdots \times_\mathrm{n} \mathbf{V}_\mathrm{n}^{1\mathrm{T}},\ [\mathrm{J}_1^\mathrm{T}, \cdots, \mathrm{J}_\mathrm{I}^\mathrm{T}] * \mathcal{X} = \mathcal{Z}_2 \times_1 \mathbf{V}_1^{2\mathrm{T}} \cdots \times_\mathrm{n} \mathbf{V}_\mathrm{n}^{2\mathrm{T}} \text{ and } \Omega(\mathcal{X}) = \Omega(\mathcal{X}_0)$$

Biao Xiong#, Qiegen Liu#, J. Xiong, S. Li, S. Wang, Dong Liang*, Field-of-Experts Filters Guided Tensor Completion, ***IEEE Transactions on Multimedia***, 20(9): 2316-2329, 2018.

Field-of-Experts Filters Guided Tensor Completion

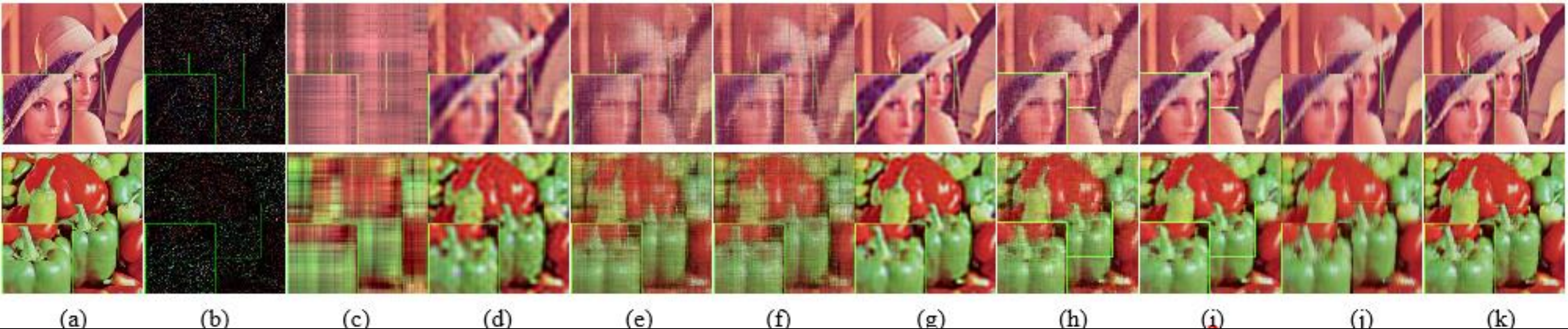

(a) Original image. (b) Observed data. (c) M²SA. (d) M²SA-G. (e) LRTC. (f) HaLRTC. (g) STDC. (h) SPCTV. (i) SPCQV. (j) FoE-LRTC. (k) FoE-STDC.

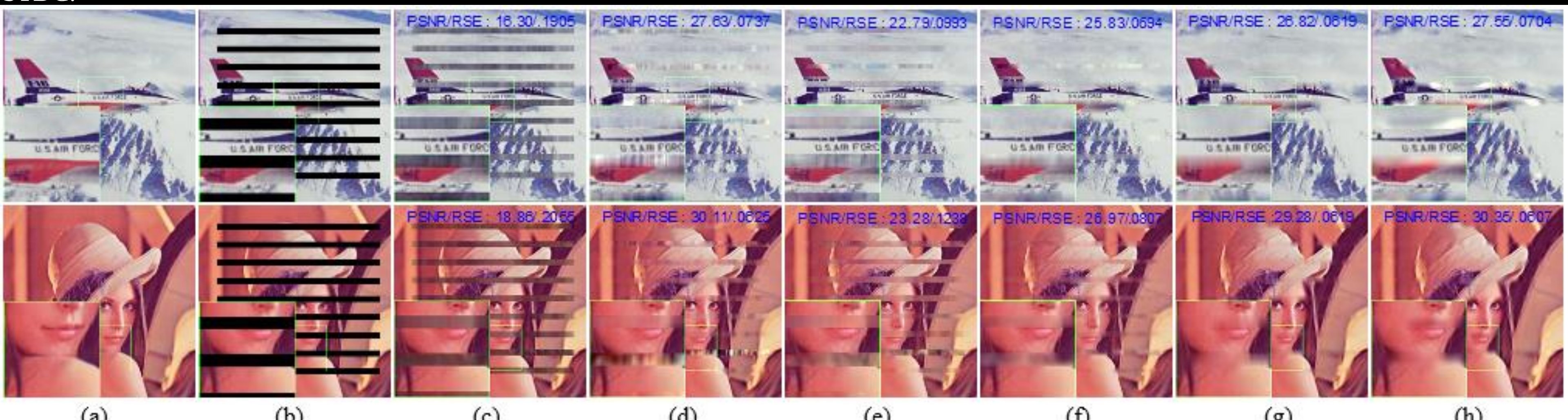

(a) Original image. (b) Observed data. (c) LRTC. (d) STDC. (e) SPCTV. (f) SPCQV. (g) FoE-LRTC. (h) FoE-STDC.

Biao Xiong#, Qiegen Liu#, J. Xiong, S. Li, S. Wang, Dong Liang*, Field-of-Experts Filters Guided Tensor Completion, ***IEEE Transactions on Multimedia***, 20(9): 2316-2329, 2018.

MF-LRTC (Multi-filters guided low-rank tensor coding)

Motivation:

- ❑ Reduce the redundancy between feature vectors at neighboring locations.
- ❑ Improve the efficiency of the overall sparse representation.

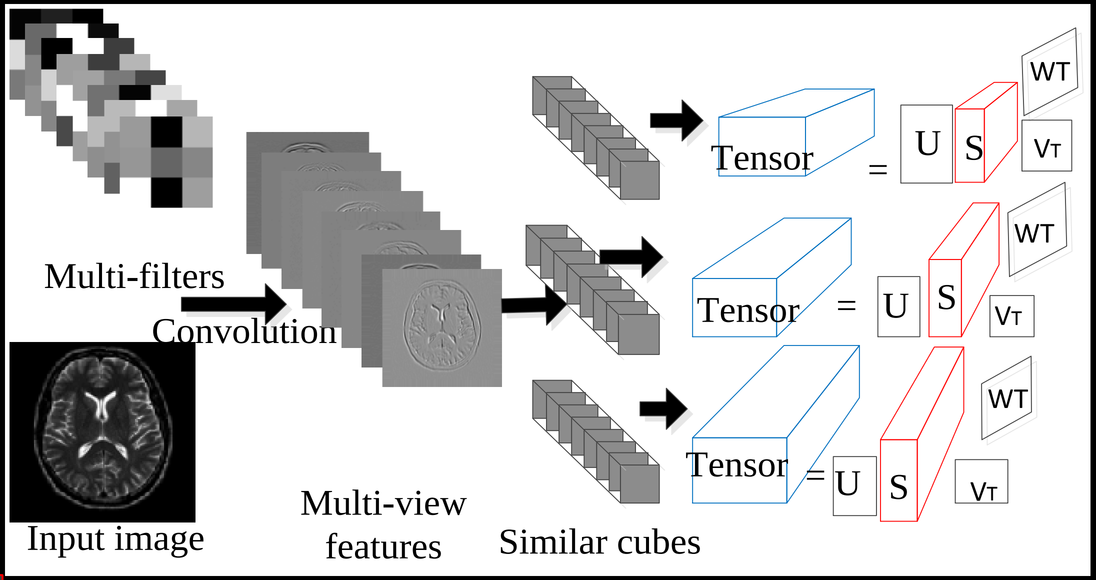

Model:

- ❑ Observed data: $y = Au + n$

A is measurement operator and *n* is noise.

- ❑ The recovery of u from y can be achieved by:

Exploration of multi-filters guided low-rank tensor coding for image restoration

$$\{u, \mathcal{Y}\} = \arg\min_{u,\mathcal{Y}} \sum_{i=1}^{N} \left\{ \frac{1}{2} \left\| \tilde{\mathbf{R}}_i [J_1^T u, \cdots, J_K^T u] - \mathcal{Y}_i \right\|_2^2 + \tau\, rank\left(\mathcal{Y}_i\right) \right\} + \frac{\nu_2}{2} \left\| y\text{-}Au \right\|_2^2$$

H. Lu, S. Li, **Q. Liu***, M. Zhang, "MF-LRTC: Multi-filters guided low-rank tensor coding for image restoration," ***Neurocomputing***, vol. 303, pp. 88-102, 2018.

MF-LRTC (Multi-filters guided low-rank tensor coding)

Image Deblurring

PSNR results of five methods at Gaussian blur kernel with different noise levels (top line: std=sqrt(1); bottom line: std=2)

Test image	TV	L0-Abs	Bayesian-TV	ASDS-TD2	MF-LRTC
Cameraman	23.08	23.51	22.59	23.90	**25.83**
	22.93	23.25	22.36	23.76	**24.82**
Peppers	25.96	26.61	24.94	26.79	**27.69**
	25.72	26.24	24.38	26.06	**26.97**

CS Recovery

Reconstruction PSNR values of four methods at un-der-sampling percentages with 63%, 73%, and 80%

	Test image	under-sampling ratio	DLMRI	Grad-DL	NLR-CS-base	MF-LRTC
2D Random	T2axialbrain	63%	38.52	43.75	48.72	**48.81**
		73%	36.77	40.84	45.22	**45.43**
		80%	35.22	38.42	42.26	**42.95**
	Herniateddisclspine	63%	39.45	42.21	46.53	**47.60**
		73%	37.40	39.67	43.28	**44.60**
		80%	35.64	37.33	39.31	**41.47**
Pseudo Radial	T2axialbrain	63%	36.68	39.54	42.96	**44.01**
		73%	34.87	36.65	39.24	**39.55**
		80%	32.75	33.88	36.31	**36.73**
	Herniateddisclspine	63%	36.77	37.08	42.83	**43.55**
		73%	34.92	34.85	38.90	**39.12**
		80%	33.03	32.30	35.44	**35.99**

H. Lu, S. Li, **Q. Liu***, M. Zhang, "MF-LRTC: Multi-filters guided low-rank tensor coding for image restoration," ***Neurocomputing***, vol. 303, pp. 88-102, 2018.

Part II-1 –Multi-channel and Multi-model based Autoencoding Prior for Grayscale Image Restoration

Algorithm overview

- Multi-channel learning scheme $\{I(u)=[u,u,u]\} \subset \{I \mid I=[I_r, I_g, I_b]\}$

Training images:

$$\{I \mid I=[I_r, I_g, I_b]\}$$

Testing stage:

$$I^k=[u^k, u^k, u^k]$$

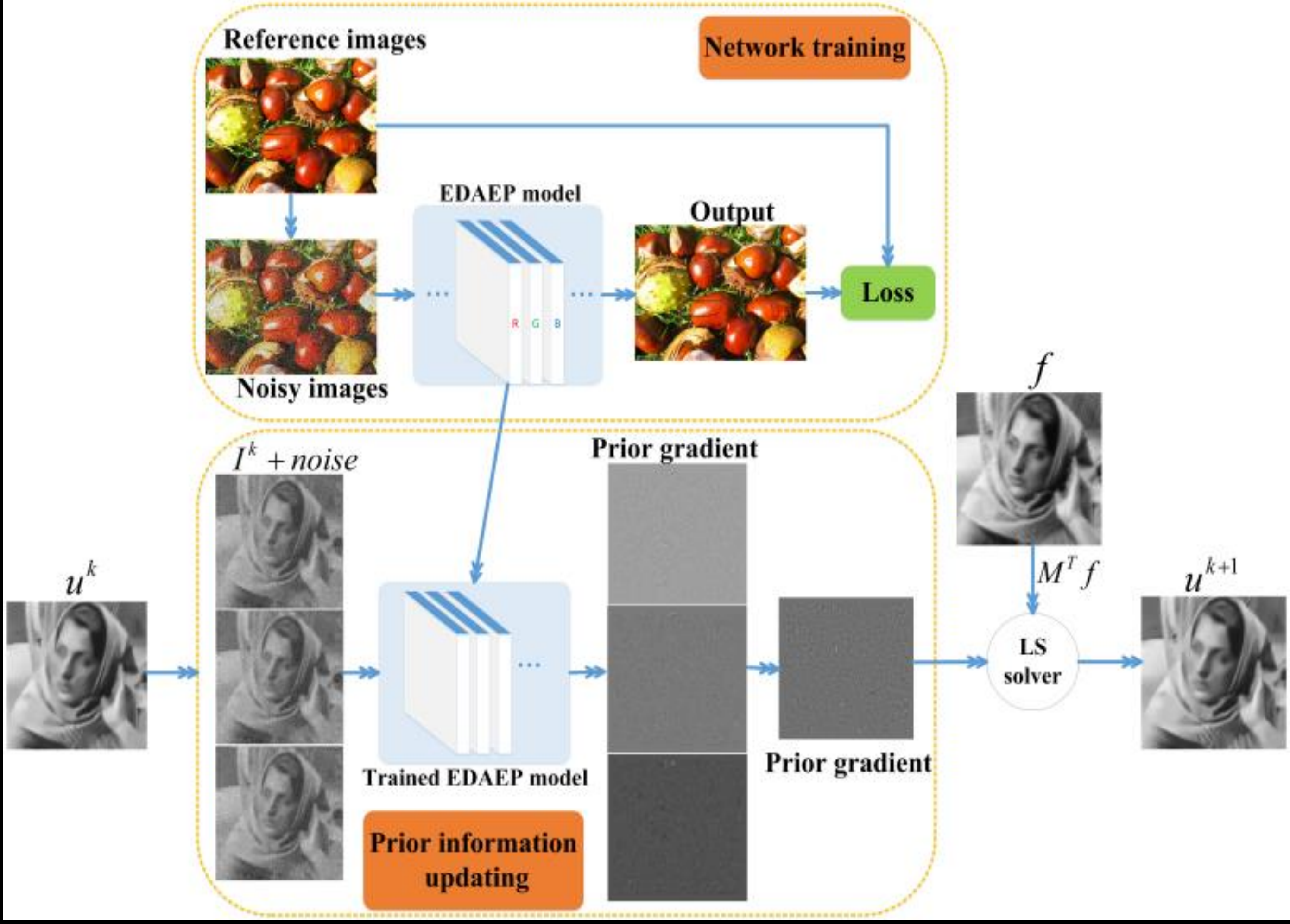

S. Li, B. Qin, Q. Liu*, Y. Wang, D. Liang*, Multi-channel and multi-model based autoencoding prior for grayscale image restoration, *IEEE Trans. Image Process.*, vol. 29, 142-156, 2020.

Algorithm overview

- Multi-model strategy

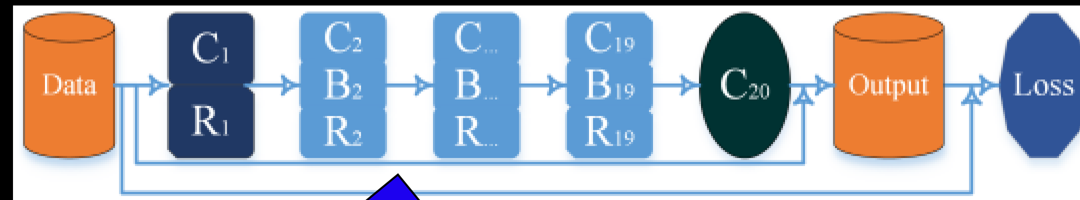

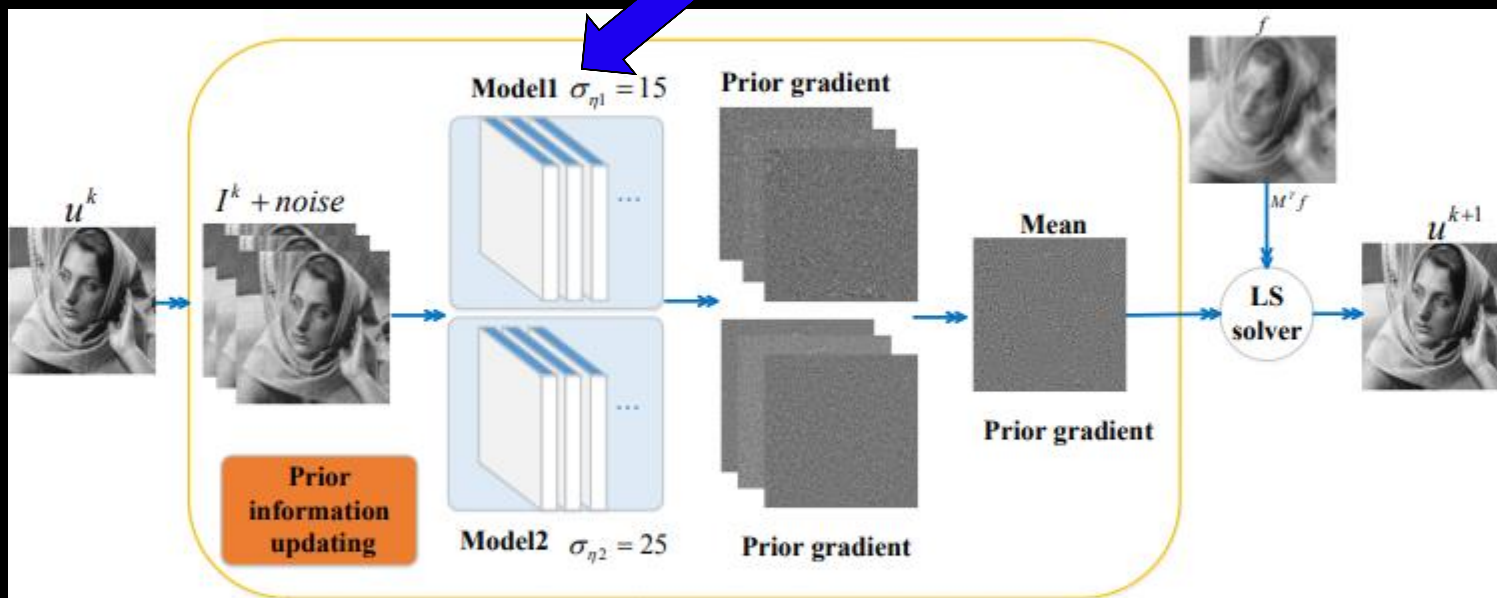

Mathematical model for IR is: $\min_u \|Mu - f\|^2 + \frac{\lambda}{N}\sum_{i=1}^{N}\left\|I(u) - A_{\sigma_{\eta i}}(I(u))\right\|^2, \quad N = 2$

S. Li, B. Qin, Q. Liu*, Y. Wang, D. Liang*, Multi-channel and multi-model based autoencoding prior for grayscale image restoration, *IEEE Trans. Image Process.*, vol. 29, 142-156, 2020.

Theoretical analysis

- The autoencoder error $A_{\sigma_\eta}(u)-u$ is proportional to the gradient of the log likelihood of the smoothed:

$$A_{\sigma_\eta}(u)-u=\sigma_\eta^2\nabla\log[g_{\sigma_\eta}*q](u)$$

where the data distribution is $Probability(u)=\int q(u+\eta)d\eta$

- The autoencoder error $A_{\sigma_\eta}(I)-I$ is proportional to the gradient of the log likelihood of the smoothed:

$$A_{\sigma_\eta}(I)-I=\sigma_\eta^2\nabla\log[g_{\sigma_\eta}*q](I)$$

where the data distribution is $Probability(I)=\int q(I+\eta)d\eta$

The effectiveness of prior (i.e., the autoencoder error) depends on the distribution of training data!

S. Li, B. Qin, Q. Liu*, Y. Wang, D. Liang*, Multi-channel and multi-model based autoencoding prior for grayscale image restoration, *IEEE Trans. Image Process.*, vol. 29, 142-156, 2020.

Experimental results

- ❑ Image Deblurring

Fig. 9. Deblurring comparison on image "Barbara". (a) Original image; (b) Noisy and blurred image (Gaussian kernel: 19 × 19, $\delta_e = 2.25$); Re[illegible] (c) LevinSps (PSNR=30.14dB; SSIM=0.885), (d) EPLL (PSNR=28.21dB; SSIM=0.904), (e) DMSP (PSNR=28.78dB; SSIM=0.897), (f) DPE (PSNR=[illegible].94dB; SSIM=0.889), (g) DAEP (PSNR=28.50dB; SSIM=0.798), (h) EDAEP (PSNR=31.83dB; SSIM=0.910) and (i) MEDAEP (PSNR=**31.88dB**; SSIM=**0.912**).

- ❑ Image Deblocking

Fig. 13. Visual comparison of image deblocking for "Womanhat" in the case of QF = 10. (a) Original image, (b) JPEG compressed image (30.49, 28.18, 0.772), (c) CONCOLOR (**31.89**, 0.815, **31.89**), (d) ARCNN (31.71, 0.810, 31.59), (e) DnCNN-3 (31.49, 0.803, 31.49), (f) MEDAEP (31.72, **0.817**, 31.67).

S. Li, B. Qin, Q. Liu*, Y. Wang, D. Liang*, Multi-channel and multi-model based autoencoding prior for grayscale image restoration, *IEEE Trans. Image Process.*, vol. 29, 142-156, 2020.

Part II-2 –Undersampled MRI Reconstruction using Autoencoding Priors

Q. Liu, Q. Yang, H. Cheng, S. Wang, M. Zhang, D. Liang*, Highly undersampled magnetic resonance imaging reconstruction using autoencoding priors, *Magn. Reson. Med.*, vol. 83, no. 1, pp. 322-336, 2020.

Algorithm overview

❑Multi-channel learning scheme (self-copy)

Training stage:

$$\{U = [u, u, u]\}$$

Testing stage:

$$U^k = [u^k, u^k, u^k]$$

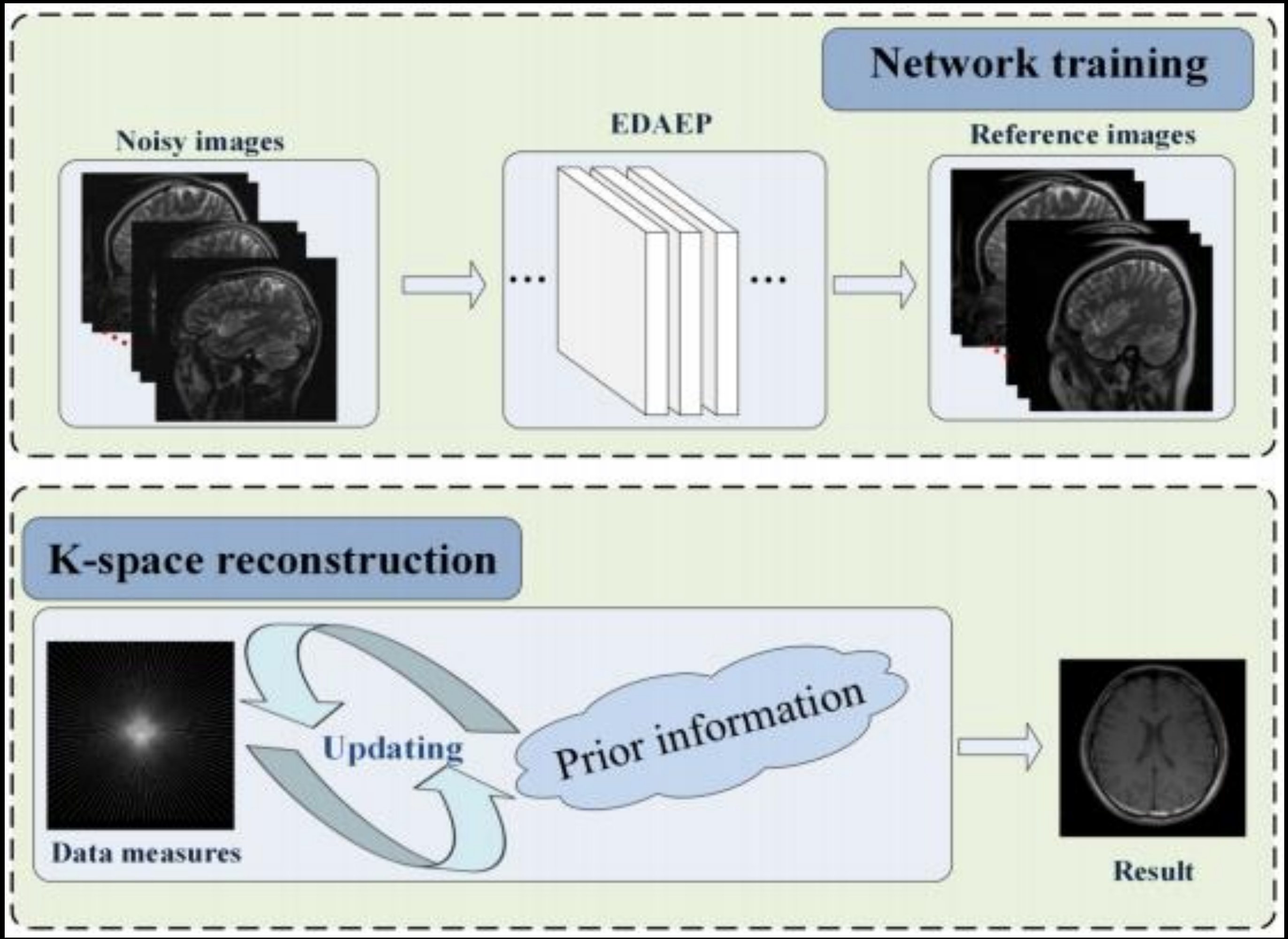

Q. Liu, Q. Yang, H. Cheng, S. Wang, M. Zhang, D. Liang*, Highly undersampled magnetic resonance imaging reconstruction using autoencoding priors, *Magn. Reson. Med.*, vol. 83, no. 1, pp. 322-336, 2020.

Algorithm overview

❑ Multi-channel learning scheme (self-copy)

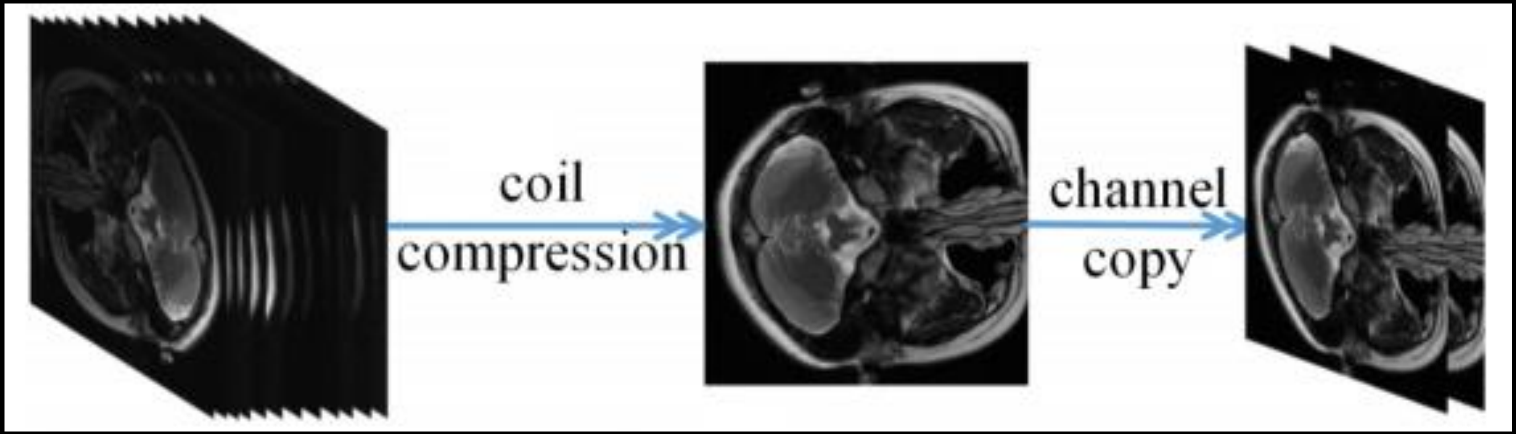

Schematic illustration of generating the three-channel training data.

Mathematical model for MRI Recon is:

$$\underset{u}{\mathrm{Min}} \frac{1}{2}\left\| U - D_{\sigma_{\eta 1}}(U) \right\|^2 + \frac{1}{2}\left\| U - D_{\sigma_{\eta 2}}(U) \right\|^2 + \nu \left\| F_p u - f \right\|^2$$

We convert the input of EDAEP from $C^{m\times n\times 3}$ space into $R^{m\times n\times 6}$ space.

Q. Liu, Q. Yang, H. Cheng, S. Wang, M. Zhang, D. Liang*, Highly undersampled magnetic resonance imaging reconstruction using autoencoding priors, *Magn. Reson. Med.*, vol. 83, no. 1, pp. 322-336, 2020.

Theoretical analysis

❑ Step1: Rate-optimal Bound on Deep-prior based Denoisers

Heckel *et al.* analytically quantified the recovery performance of deep-prior based denoisers. Given a *d*-layer generative neural network $G: R^S \to R^N$ with $S < N$ and random weights, the authors presented a gradient method with a tweak that aims to minimize the last-square loss $\|G(x)-y\|^2$ between the corrupted image y and the network output $G(x)$. They proved that the proposed algorithm yields an estimate $\hat{x}$ obeying:

$$\|G(\hat{x})-y_*\|^2 \lesssim \sigma^2 \frac{S}{N}$$

❑ Step2: Experimental Comparisons of Learned Prior on 1-channel and 3-channel Data

Various *S*-value

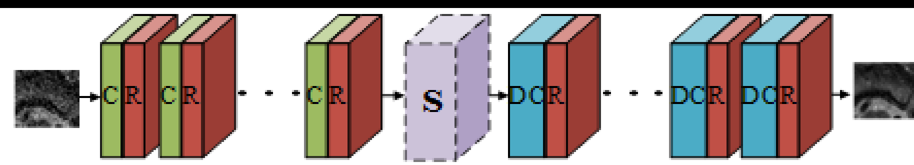

Figure S1_2. The architecture of DWTA-1 network. Each convolutional/deconvolutional layer is followed by its rectified linear units (ReLU). The channel number is 1 at input and output layer, and 64 for the rest of the layers. C, DC, R and S represent convolutional, deconvolutional, ReLU layers and Sparse, respectively.

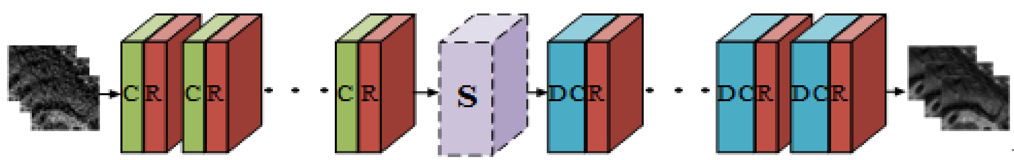

Figure S1_3. The architecture of DWTA-3 network. Each convolutional/deconvolutional layer is followed by its rectified linear units (ReLU). The channel number is 3 at input and output layer, and 64 for the rest of the layers. C, DC, R and S represent convolutional, deconvolutional, ReLU layers and Sparse, respectively.

Q. Liu, Q. Yang, H. Cheng, S. Wang, M. Zhang, D. Liang*, Highly undersampled magnetic resonance imaging reconstruction using autoencoding priors, *Magn. Reson. Med.*, vol. 83, no. 1, pp. 322-336, 2020.

Theoretical analysis

❑ Step2: Experimental Comparisons of Learned Prior on 1-channel and 3-channel Data

Various *S*-value

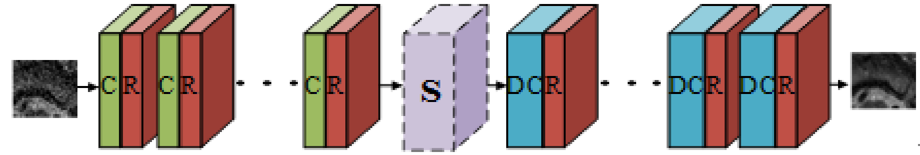

Figure S1_2. The architecture of DWTA-1 network. Each convolutional/deconvolutional layer is followed by its rectified linear units (ReLU). The channel number is 1 at input and output layer, and 64 for the rest of the layers. C, DC, R and S represent convolutional, deconvolutional, ReLU layers and Sparse, respectively.

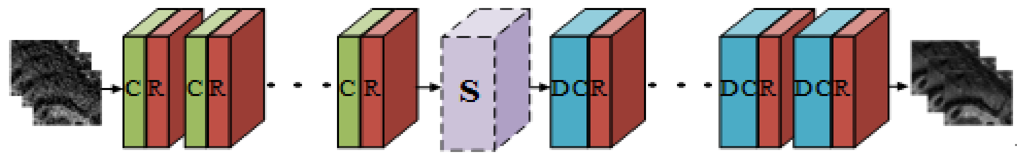

Figure S1_3. The architecture of DWTA-3 network. Each convolutional/deconvolutional layer is followed by its rectified linear units (ReLU). The channel number is 3 at input and output layer, and 64 for the rest of the layers. C, DC, R and S represent convolutional, deconvolutional, ReLU layers and Sparse, respectively.

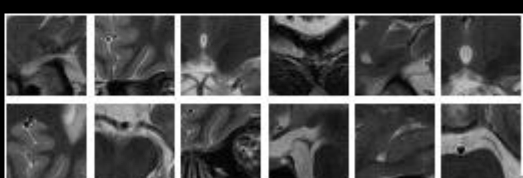

Set12 test images used for image recovery from noise corrupted images.

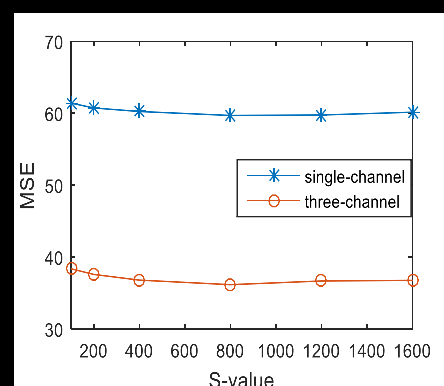

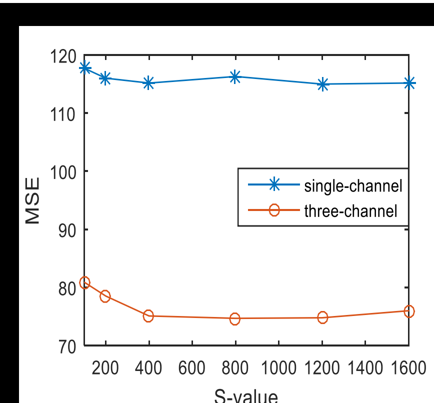

Average MSE values *vs. S*-sparse values in DWTA-1 and DWTA-3 network at noise level of (a) 15 and (b) 25 conducted on Set 12.

Q. Liu, Q. Yang, H. Cheng, S. Wang, M. Zhang, D. Liang*, Highly undersampled magnetic resonance imaging reconstruction using autoencoding priors, *Magn. Reson. Med.*, vol. 83, no. 1, pp. 322-336, 2020.

Experimental results

Average PSNR, SSIM and HFEN values (mean ± std) of reconstructing 31 test images.

(a)	DLMRI	PANO	FDLCP	NLR-CS	DC-CNN	DAEPRec	EDAEPRec
R=3.3	33.43(±0.87) 0.9054(±0.0101) 0.63(±0.0544)	34.64(±1.26) 0.9152(±0.0161) 0.56(±0.0799)	34.89(±1.20) 0.9135(±0.0170) 0.50(±0.0670)	35.31(±1.48) 0.9099(±0.2333) 0.47(±0.0778)	**35.71(±1.38)** 0.9234(±0.0176) 0.44(±0.0659)	34.04(±1.00) 0.9111(±0.0122) 0.62(±0.0589)	35.62(±1.16) **0.9279(±0.0130)** **0.42(±0.0676)**
R=4	32.41(±0.87) 0.8866(±0.0113) 0.84(±0.0852)	33.65(±1.23) 0.8995(±0.0180) 0.73(±0.0999)	34.04(±1.18) 0.8980(±0.0196) 0.62(±0.0821)	34.35(±1.43) 0.8938(±0.0256) 0.61(±0.0950)	34.07(±1.26) 0.8992(±0.0256) 0.69(±0.0950)	33.21(±0.98) 0.8973(±0.0135) 0.76(±0.0695)	**34.49(±1.15)** **0.9151(±0.0146)** **0.64(±0.0822)**
R=5	31.21(±0.83) 0.8602(±0.0135) 1.10(±0.0933)	32.44(±1.16) 0.8777(±0.0194) 0.96(±0.1217)	32.97(±1.16) 0.8770(±0.224) 0.80(±0.1037)	33.32(±1.24) 0.8812(±0.0243) 0.79(±0.1119)	32.68(±1.10) 0.8791(±0.0243) 0.95(±0.1119)	32.29(±0.96) 0.8797(±0.0150) 0.94(±0.0840)	**33.49(±1.14)** **0.8990(±0.0167)** **0.79(±0.1015)**
R=10	27.39(±0.98) 0.7444(±0.0288) 2.18(±0.2198)	28.58(±1.00) 0.7805(±0.0254) 1.90(±0.2014)	29.34(±1.13) 0.7856(±0.0333) 1.60(±0.2008)	29.51(±1.16) 0.7845(±0.0243) 1.65(±0.2140)	28.39(±0.93) 0.7710(±0.0243) 1.93(±0.2140)	29.65(±0.94) 0.8160(±0.0213) 1.56(±0.1469)	**30.30(±1.17)** **0.8319(±0.0254)** **1.40(±0.1842)**
(b)	DLMRI	PANO	FDLCP	NLR-CS	DC-CNN	DAEPRec	EDAEPRec
R=6.7, 2D Random	27.63(±0.98) 0.7518(±0.0257) 2.02(±0.1849)	29.12(±1.06) 0.7964(±0.0243) 1.77(±0.1976)	30.14(±1.19) 0.8004(±0.0328) 1.44(±0.1890)	30.34(±1.21) 0.8087(±0.0327) 1.46 (±0.1992)	28.78(±1.02) 0.7873(±0.0327) 1.83(±0.1992)	29.90(±0.91) 0.8232(±0.0201) 1.49(±0.1312)	**30.68(±1.20)** **0.8433(±0.0258)** **1.31(±0.1921)**
R=6.7, Pseudo Radial	29.36(±0.99) 0.8103(±0.0243) 1.58 (±0.1991)	30.60(±1.12) 0.8372(±0.0231) 1.37(±0.1694)	31.31(±1.15) 0.8391(±0.0275) 1.13(±0.1463)	31.35(±1.05) 0.8494(±0.0232) 1.17(±0.1341)	30.57(±1.04) 0.8348(±0.0232) 1.38(±0.1341)	30.99(±0.96) 0.8512(±0.0177) 1.22(±0.1102)	**32.00(±1.19)** **0.8716(±0.0213)** **1.05(±0.1470)**
R=6.7, 1D Cartesian	26.50(±1.08) 0.7390(±0.0416) 2.51(±0.2223)	27.51(±0.98) 0.7683(±0.0320) 2.28(±0.2214)	27.91(±1.07) 0.7776(±0.0335) 2.15(±0.2448)	28.23(±1.10) 0.7798(±0.0361) 2.03(±0.2391)	27.05(±0.89) 0.7506(±0.0361) 2.44(±0.2391)	28.67(±1.20) 0.8012(±0.0304) 1.86(±0.2526)	**28.85(±1.32)** **0.8041(±0.0348)** **1.81(±0.2807)**

Q. Liu, Q. Yang, H. Cheng, S. Wang, M. Zhang, D. Liang*, Highly undersampled magnetic resonance imaging reconstruction using autoencoding priors, *Magn. Reson. Med.*, vol. 83, no. 1, pp. 322-336, 2020.

Experimental results

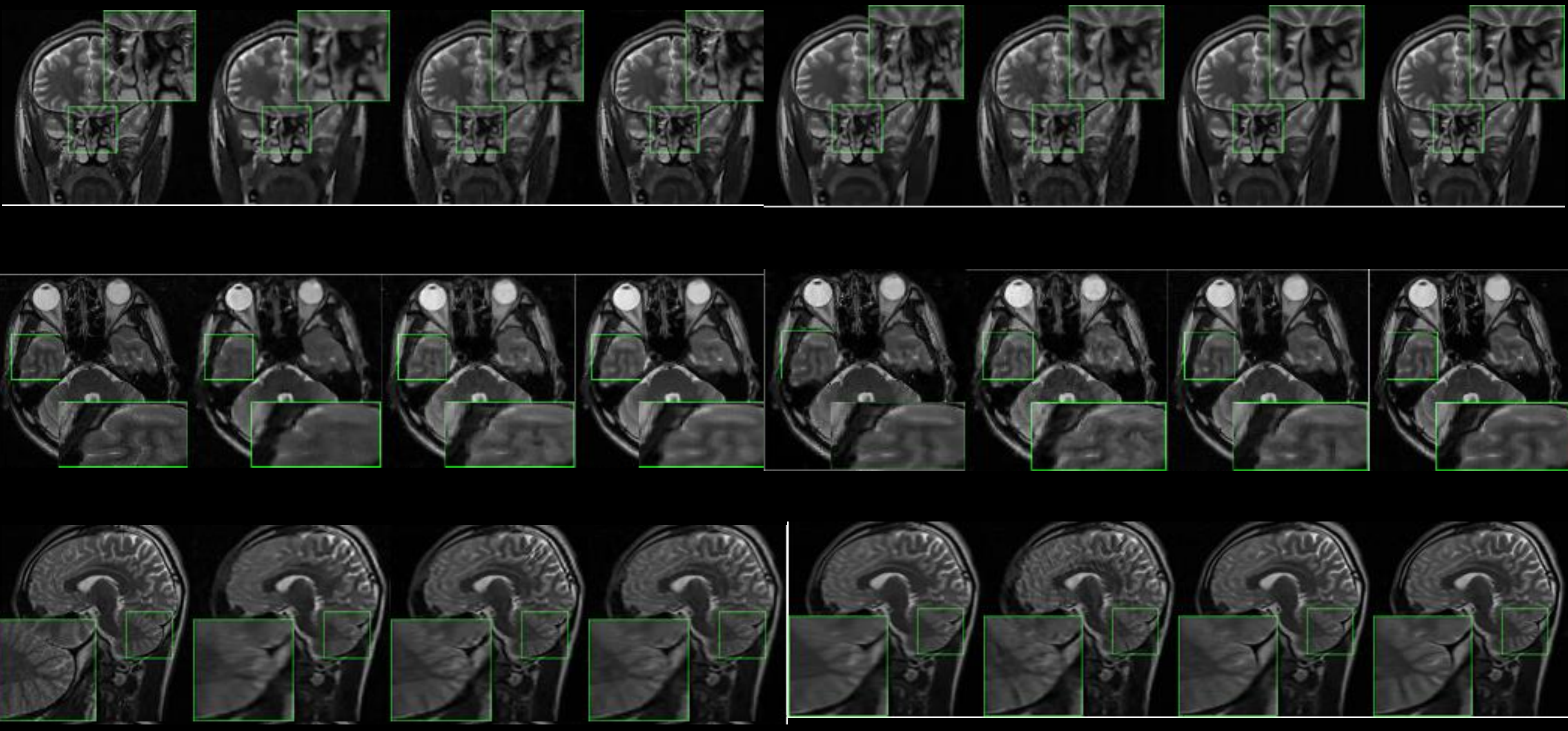

Q. Liu, Q. Yang, H. Cheng, S. Wang, M. Zhang, D. Liang*, Highly undersampled magnetic resonance imaging reconstruction using autoencoding priors, *Magn. Reson. Med.*, vol. 83, no. 1, pp. 322-336, 2020.

Part II-3 – Sparse-view CT Reconstruction via Robust and Multi-channels Autoencoding Priors

Priors learning procedure

- At the prior learning stage, we train a three-channels network with input-output pairs of the ground-truth color natural image and its noisy version, the EDAEP prior can be denoted as: $L_{EDAE} = E_{\eta,U}[\|U - A_{\sigma_\eta}(U)\|^2]$

  where the training dataset is $\{U \mid U = [U_r, U_g, U_b]\}$

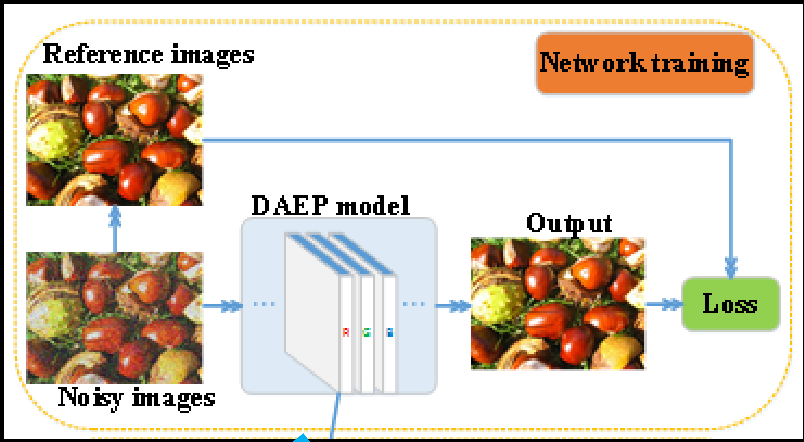

- The joint learning of the (R, G, B)-channel noisy images exhibits structural information, due to the inherent channel priors.

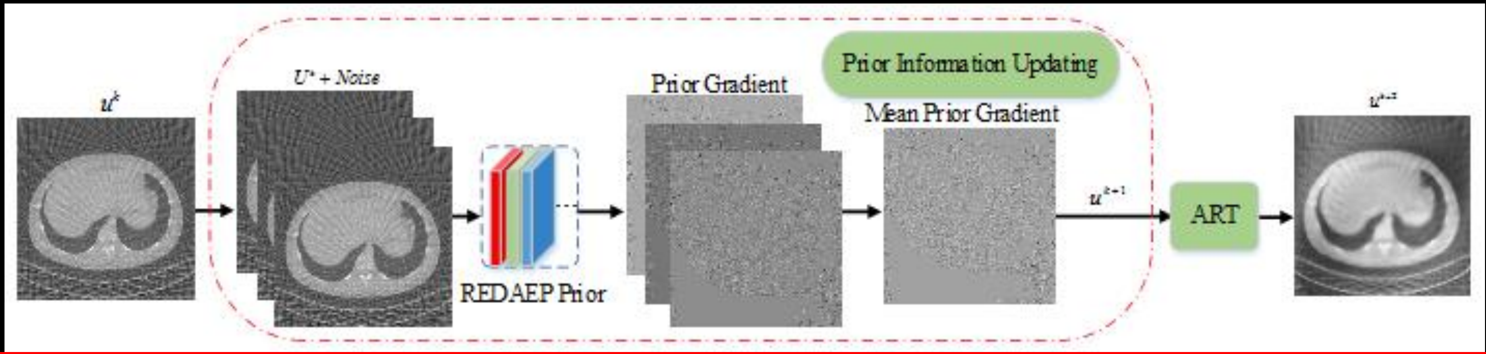

M. Zhang, F. Zhang, Q. Liu and D. Liang, Sparse-View CT reconstruction via Robust and Multi-channels Autoencoding Priors, ISICDM 2018, Chengdu, China.

CT reconstruction procedure

- After the prior is learned, the mathematical reconstruction model can be achieved by solving the following minimization:

$$\min_u \|Mu - f\|^2 + \lambda \|U - A_{\sigma_\eta}(U)\|^p$$

here the auxiliary variable $U = [u, u, u]$ is caused from the desired solution variable u.

- The testing samples space falls into the learning samples space, i.e.,

$$\{U = [u, u, u]\} \subset \{U \mid U = [U_r, U_g, U_b]\}$$

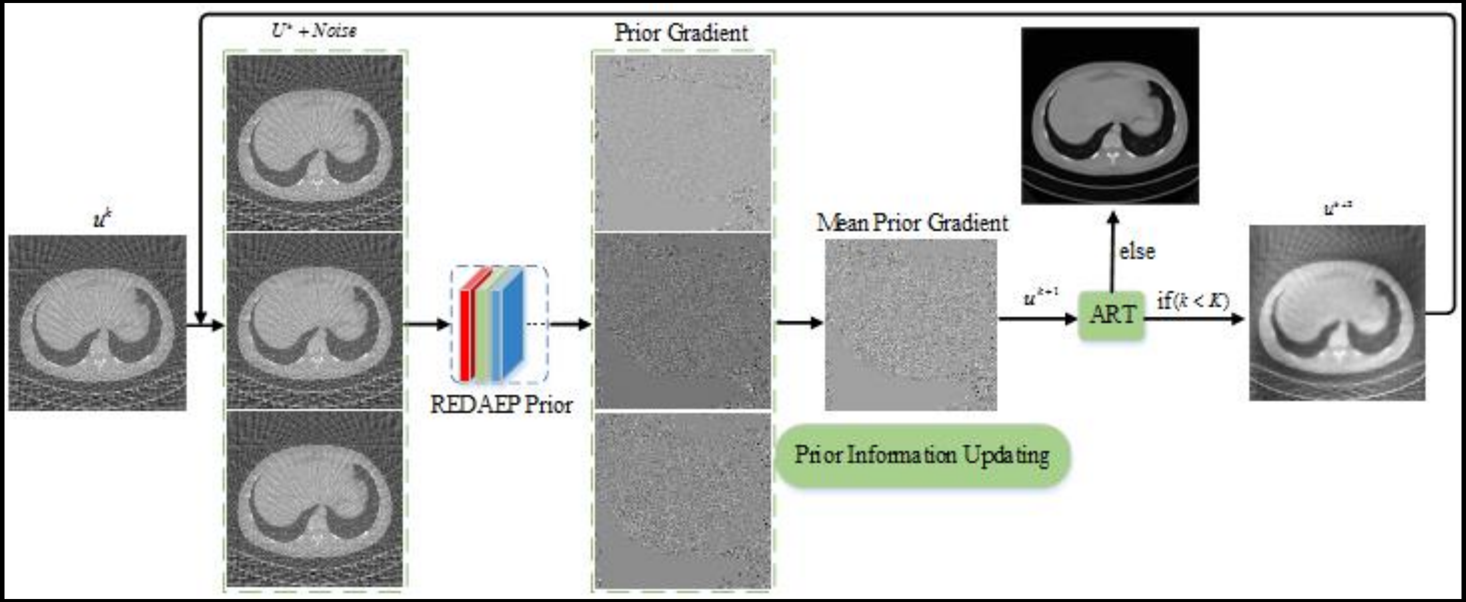

Schematic flowchart of REDAEP algorithm for CT reconstruction.

M. Zhang, F. Zhang, Q. Liu and D. Liang, Sparse-View CT reconstruction via Robust and Multi-channels Autoencoding Priors, ISICDM 2018, Chengdu, China.

Algorithm

Algorithm 1 REDAEP

Initialization: $u^0 = M^T f$

Loop #iterations $k = 1, 2, \cdots, K$

1: Add the auxiliary variable $U^k = [u^k, u^k, u^k]$;

2: Compute the gradient of REDAEP term:

$$\nabla_U G^k = \frac{1}{\left| U^k - A_{\sigma_\eta}(U^k) \right|} \circ [\nabla_U A^T_{\sigma_\eta}(U^k)[A_{\sigma_\eta}(U^k) - U^k] + U^k - A_{\sigma_\eta}(U^k)];$$

3: $U^{k+1} = U^k - \gamma \nabla_U G^k$; $u^{k+1} = Mean(U^{k+1})$;

4: Compute the gradient of data-fidelity term (ART iteration):

5: $u^{k+2} = u^{k+1} + \beta M_i \dfrac{f_i - M_i u^{k+1}}{\|M_i\|^2}$, $i = 1, \cdots, I$;

End loop

Regularization term

Data-fidelity term

The overall testing phase of REDAEP algorithm ($p = 1$).

M. Zhang, F. Zhang, Q. Liu and D. Liang, Sparse-View CT reconstruction via Robust and Multi-channels Autoencoding Priors, ISICDM 2018, Chengdu, China.

Experiments

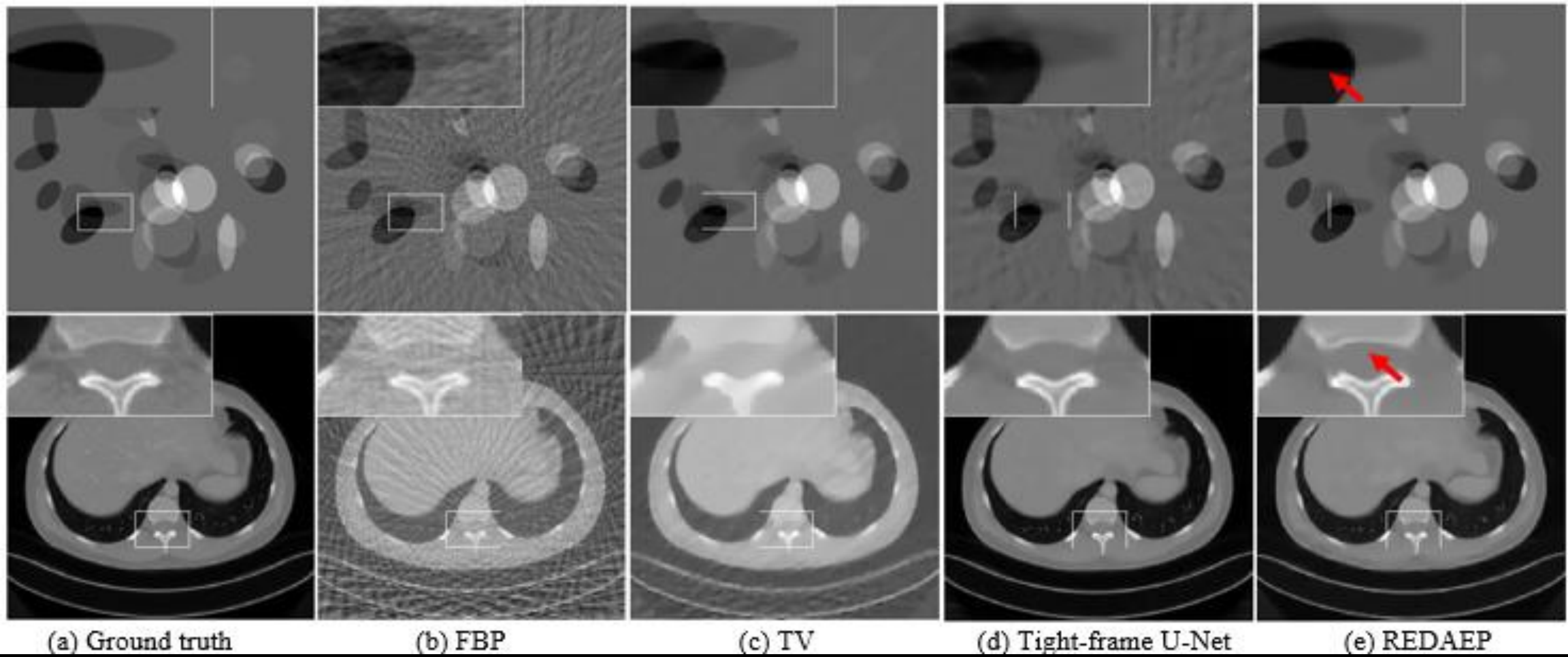

Reconstructed images of simulated ellipsoidal and real CT1 data from 60 views using FBP, TV, Tight-frame U-Net and the proposed REDAEP.

M. Zhang, F. Zhang, Q. Liu and D. Liang, Sparse-View CT reconstruction via Robust and Multi-channels Autoencoding Priors, ISICDM 2018, Chengdu, China.

Experiments and Summary

Reconstruction PSNRs/SSIMs of numerical ellipsoidal data and real CT data.

Views	Images	TV	Tight-frame U-Net	REDAEP
60	Ellipsoid	40.61/0.9786	33.25/0.9563	**45.00/0.9853**
	CT1	30.33/0.8470	38.92/0.9354	38.27/**0.9470**
120	Ellipsoid	44.56/0.9877	38.85/0.9779	**48.09/0.9889**
	CT2	36.93/0.9056	41.17/0.9453	**41.23/0.9556**

Summary :

- A multi-channels network for single-channel CT reconstruction is proposed. The principle is to exploit high-dimensional structural prior via enhancing the DAE priors.

- We modify the objective function in the basic DAEP model from L2-norm to L1-norm. Subsequently, it provides the reconstructions with more texture details.

M. Zhang, F. Zhang, Q. Liu and D. Liang, Sparse-View CT reconstruction via Robust and Multi-channels Autoencoding Priors, ISICDM 2018, Chengdu, China..

Part III –
Summary and Conclusions

Today We Have Seen that …

Two successful applications in decolorization and IR problem

Motivation

Metrics or/and learning in higher-dimensional data space is better for data representation

Apply to Rec via enhanced DAEP?

Color prior

Self-copy prior

Robust p-norm prior

Applications of deep learning

Grayscale IR

MRI reconstruction

Sparse-View CT Reconstruction

More details (including the papers and relevant codes) can be found in http://www.escience.cn/people/liuqiegen/index.html; https://github.com/yqx7150

Code：

http://www.escience.cn/people/liuqiegen

https://github.com/yqx7150

Qiegen Liu (刘且根)

Nanchang University， Associate professor

研究兴趣： Dictionary learning , compressed sensing , Image Processing , Deep l

Love to imaging science!

Code

Code of TDAEP (Transformed Denoising Autoencoding Priors for Imaging Inverse Problems)

Code of MWDMSP (Multi-Wavelet Guided Deep Mean-shift Prior for Image Restoration)

Code of M2DAEP (High-dimensional embedding denoising autoencoding prior for color Image restoration)

Code of MEDAEP (Multi-channels and Multi-models based Autoencoding Priors for Grayscale Image Restoration)

Code of VST-Net (VST-Net: Variance-stabilizing Transformation Inspired Network for Poisson Denoising)

Code of EDAEPRec (Highly Undersampled Magnetic Resonance Imaging Reconstruction using Autoencoding Priors)

Code of RicianNet (Progressively distribution-based Rician noise removal for magnetic resonance imaging)

Code of MDAEP-SR (Learning Multi-Denoising Autoencoding Priors for Image Super-Resolution)

Code of Iterative-scheme Inspired Network (Iterative-scheme Inspired Network for Impulse Noise Removal)

Matlab code of MFLRTC_inpainting (Multi-filters guided low-rank tensor coding for image inpainting)

Matlab code of Dictionary Learning (predual dictionary learning (PDL) / augmented Lagrangian multi-scale dictionary learning(ALI

信息工程学院
School of Information Engineering

Thanks all!

And also thanks MICS-2019 organizers,
Zhipei Liang, Dong Liang, Henry Leung, Shanshan Wang, Minghui Zhang, Yuhao Wang, Binjie Qin and master students Hongyang Lu, Jiaojiao Xiong, Sanqian Li, Fengqin Zhang, Qinxin Yang, Wenzhao Zhao